Jour. Fac. Sci., Hokkaido Univ., Ser. VII (Geophysics), Vol. 8, No. 1, 83-108, 1986.

Body Wave Analyses of Strain Seismograms Observed at Erimo, Hokkaido, Japan

Minoru Kasahara

Research Center for Earthquake Prediction, Faculty of Science, Hokkaido University, Sapporo 060, Japan

and

Tsutomu Sasatani

Department of Geophysics, Faculty of Science, Hokkaido University, Sapporo 060, Japan

(Received November 25, 1985)

Abstract

At the Erimo Geophysical Observatory (EGO) a digital recording system has been introduced on July, 1976 into the Earth strain measurements in order to use the fused-quartz extensometer of 30 m long as a seismometer. The body wave parts of the strain seismograms from 14 earthquakes with magnitudes ranging from 4.7 to 7.7 recorded by the system were compared with the synthetic strain seismograms generated by a point shear dislocation in an infinite homogeneous medium. The waveform and amplitude of the observed strain seismogram could be well explained by the synthetic one calculated for appropriate source parameters deduced from the conventional method. Based on this result it can be shown that the period of the observed S-wave approximately represents the source process time of an earthquake and the S-wave amplitude is proportional to the seismic moment of the event.

The seismic moment ($\boldsymbol{Mo}$: dgne • cm) of the earthquake can be estimated within a factor of 2 from the amplitude (e_s : 10^{-9} strain) and period (τ_e : sec) of the S-wave observed at the hypocentral distance (r : km) using the following equation, $\boldsymbol{Mo} = 4.5 \times 10^{19} \cdot e_s \cdot r\, \tau_e^2$. The source process time and seismic moment for 41 earthquakes with magnitude ranging from 3.3 to 7.3 were determined by this relation only. The relationship between both parameters obtained here for 55 earthquakes ($0.3 \leq \tau_e \leq 60$ sec and $10^{20} \leq \boldsymbol{Mo} \leq 10^{27}$ dyne • cm) is consistent with that predicted by the scaling law of the earthquake dislocation model.

1. Introduction

A pronounced availability of the extensometer as a seismometer is that it can uniformly respond to crustal movements in the frequency range from several Hz to DC without such transient characteristics as a pendulum-type

seismometer has. Recently, much attention has been given to slow earthquakes generated by a rupture process with a long time constant (Kanamori, 1972; Kanamori and Cipar, 1974; Fukao and Furumoto, 1975; Sasatani and Kasahara, 1978; Sacks et al., 1978; Chung and Kanamori, 1978; Kanamori and Stewart, 1979; Kasahara and Sasatani, 1985). For these earthquakes, usual seismometers have provided no records or incomplete records, but the extensometer could record the whole deformation caused by the rupture process. In other words, the extensometer could successfully reveal the other side of source process behind our knowledge of earthquake mechanism (Okada, 1980). However, until now, strain seismograms, especially in the parts of body waves, have not received much attention because available data for analysis of strain seismograms have been scarce. In order to analyze the observed strain seismograms, the direct records of the extensometer with a good time resolution and without any low-cut filter are required. For this reason, a digital recording system to maintain a broad bandwidth and a wide dynamic range is the best one for the extensometric observation (Berger and Wyatt, 1973).

On the telemeterization in July, 1976 for the seismic and geodetic observation network of Hokkaido University, we have introduced a digital recording system for the extensometers which have been installed in the vault of the Erimo Geophysical Observatory (EGO) in August, 1971 (Kasahara, 1976; Maeda et al., 1978). By this system 55 earthquakes with magnitude ranging from 3.3 to 7.7 and with the epicentral distance from 22 km to 1,200 km were clearly recorded during the period from July, 1976 to February, 1980. Fig. 1 shows a location of the EGO and an epicentral distribution of all, but except one, of the earthquakes, of which strain seismograms were analyzed in this study on the basis of comparison with synthetic ones generated by a double-couple point source model in an infinite, homogeneous medium. We will show that the observed strain seismograms in the initial part of the body waves are well modeled by this earthquake model and that the source parameters of the earthquake, the seismic moment and the source process time, are directly determined by the amplitude and the period of S-wave of the observed strain seismogram with the hypocentral distance.

2. Instrumentation

Fig. 2 shows a geological map around EGO (upper part) (Funahashi and Hashimoto, 1951) and a ground plane of the observational vault (lower part). The vault was newly dug in 1970 at the foot of a hill with a relative altitude of

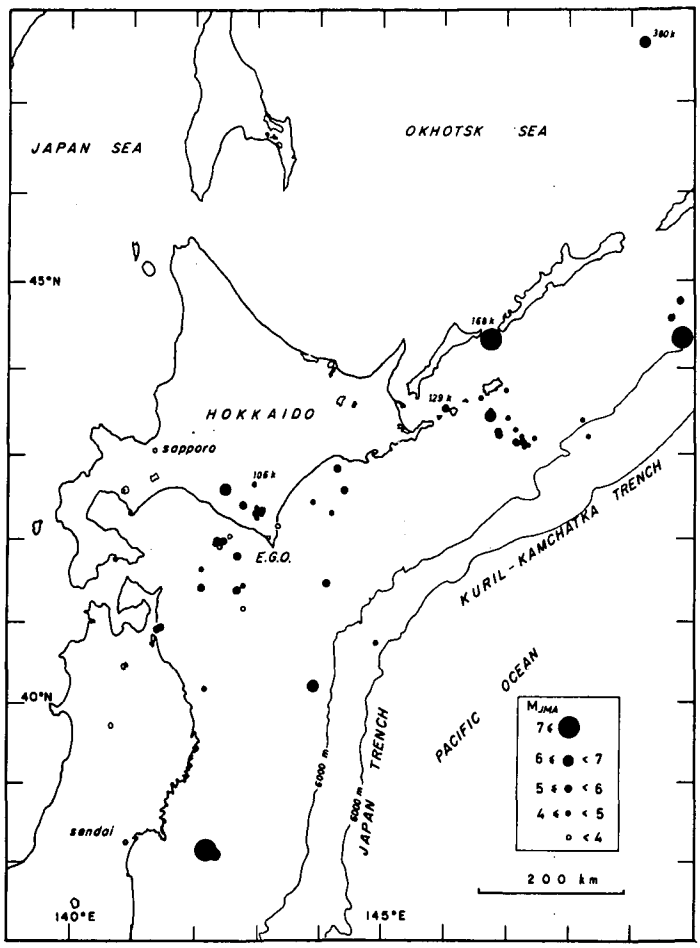

Fig. 1 Map showing the location of the Erimo Geophysical Observatory (EGO) and the epicenters of 55 earthquakes, of which strain seismograms were analyzed. For the epicenter of No. 12, see Fig. 8. The earthquake data are listed in Table 2.

about 130 meters which consists of entirely the triassic slate. The northern part of the line A-A′ as shown in this figure, which is called Horoizumi (old name of Erimo) Sheared Zone, is occupied by complex metamorphic rock. On the other hand, the southern part of this line including the vault shows uniform geological structure. In August, 1971 three components of the fused-quartz tube extensometer were installed in the vault, that is E-AB (NW-SE direction), E-CD (NE-SW direction), and E-EF (E-W direction) components as shown in

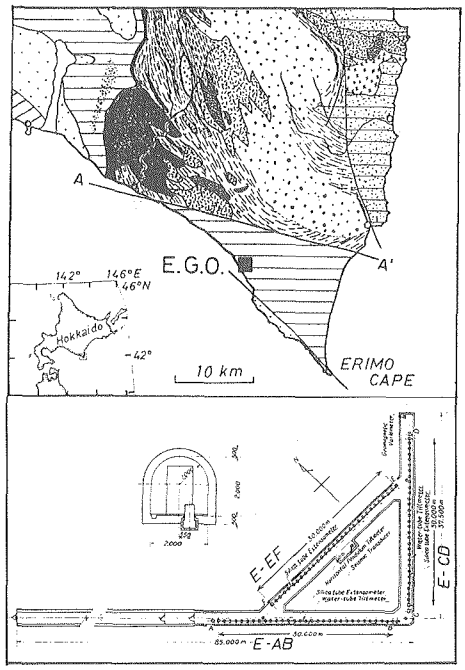

Fig. 2 Geological map around EGO (after Funahashi and Hashimoto, 1951) and horizontal cross section views of the observational vault are shown in the upper and lower parts, respectively.

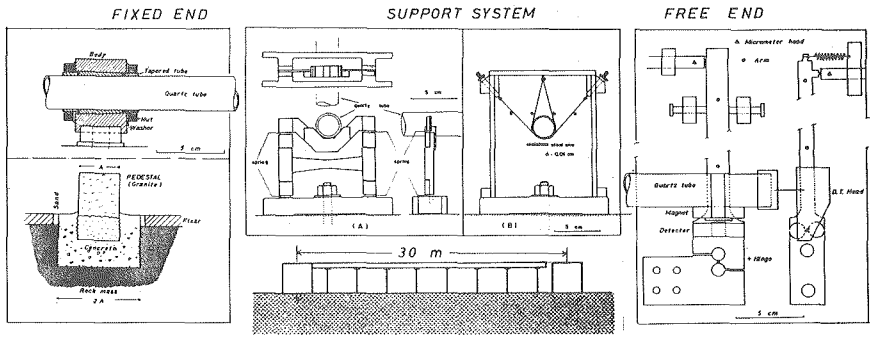

Fig. 3 Schematic diagrams showing the fixer (left), rod supporting system (middle), and free end (right). Specification for pedestal settlement is also shown (left, bottom).

the ground plane. Fig. 3 shows schematic representation of the main parts of the extensometer at EGO. The length standard is 30 meters long and is made up of 2 meter sections of milky quartz tubing 2.6 cm in outside diameter by 0.25 cm wall thickness. The sections are connected end to end by welding. The standard is fixed by fastening mechanism using a tapered iron pipe with a

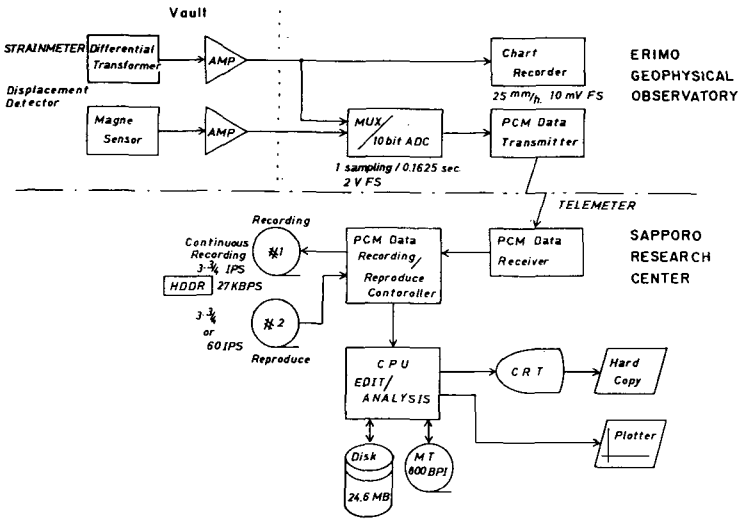

Fig. 4 Block diagram of the observational system.

narrow gap. The quartz tube is supported at one meter intervals by supporting structure, which was the inverted pendulum type (Blayney and Gilman, 1965; Okada et al., 1975) at first (Fig. 3 (A)) and is now the hanging system by double slings of stainless-steel wire 0.1 mm in diameter from the end of 1979 (Fig. 3 (B)). The latter is a slightly modified form of the Benioff's design (Benioff, 1959). The standard is covered with 5 cm thickness poly-styrene in order to deduce thermal effects resulting short term disturbances.

Fig. 4 shows a block diagram of the system for observation and recording used in the present study. A differential transformer has been used as a displacement detecter. A magnesensor is also added at the time when the sensitivity of the system is increased. Sampling frequency for the extensometer as a seismometer is provided with 6.15 Hz, because about 3 Hz is the upper limit of the observable frequency to measure a relative displacement between two points with a distortion less than 1% for the extensometer of 30 m long (Benioff, 1935). The data sampled in 10 bits linear quantization mode are transformed with non-linear quantization in 8 bits mode for transmitting and recording the data. All the data are continuously recorded on a magnetic tape through the High Density Data Recorder (Honeywell model 96).

During the period from July, 1976 to November, 1977 the data through the high-cut filter at 1 Hz were recorded with a sensitivity of 0.785×10^{-9}/bit. The sensitivity and the cut-off frequency have been varied to 1.36×10^{-9}/bit and to

0.5 Hz, respectively from March of 1978. From these conditions we could obtain the strain seismograms enough to analyze the earthquakes with magnitudes of 5 or more and with an epicentral distance of about 100 km. In addition to these channels, a high gain channel which consists of the band-pass filtered data between 3 Hz and 0.01 Hz with a sensitivity of 1.13×10^{-10}/bit has been provided for the purpose of analyzing smaller earthquakes.

3. Synthetic strain seismogram

In order to interpret the observed strain seismograms we will consider synthetic strain seismograms from an earthquake model. Appropriate source parameters will be obtained by matching them with the observed records. As the source model we will take a double-couple point source in an infinite homogeneous medium for the first approximation. It is well known that this approximation provides a good comparison of wave forms in sofar as the early parts of P- and S-waves prior to the arrival of surface waves are taken.

Let us take the Cartesian co-ordinates (x, y, z) in an infinite medium and put a double-couple point source with the moment function, $M(t)$, at the origin as shown in Fig. 5. This point source is equivalent to the shear faulting (Maruyama, 1963). Dynamic displacements (Ux, Uy, Uz) at a point (x, y, z) are given (Honda, 1962) by

$$\begin{aligned} U_x &= -\frac{Mo}{4\pi\rho}\left\{2\frac{\partial^3}{\partial x^2\partial y}(\Phi-\Psi)+\frac{\partial}{\partial y}\nabla^2\Psi\right\} \\ U_y &= -\frac{Mo}{4\pi\rho}\left\{2\frac{\partial^3}{\partial x\partial y^2}(\Phi-\Psi)+\frac{\partial}{\partial x}\nabla^2\Phi\right\} \\ Uz &= -\frac{Mo}{4\pi\rho}\left\{2\frac{\partial^3}{\partial x\partial y\partial z}(\Phi-\Psi)\right\} \end{aligned} \qquad (1)$$

where,

$$\Phi=\frac{1}{r}F(t-t_\alpha), \qquad \Psi=\frac{1}{r}F(t-t_\beta),$$

$$r=(x^2+y^2+z^2)^{1/2}, \qquad t_\alpha=\frac{r}{\alpha},\ t_\beta=\frac{r}{\beta},$$

$$F(t)=\int_0^{t'}\int_0^{t''}F''(t'')\,dt''\,dt', \quad F''(t)=\frac{1}{Mo}M(t),$$

where ρ is the density of the medium, α and β are the velocities of P- and S-waves and Mo is the final seismic moment. The spatial differentiation of these displacements may give the dynamic strain fields, e_{ij}.

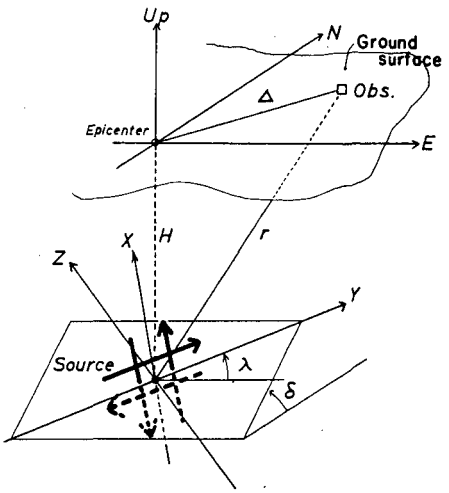

Fig. 5 Geometry of an arbitrarily oriented buried double-couple point source.

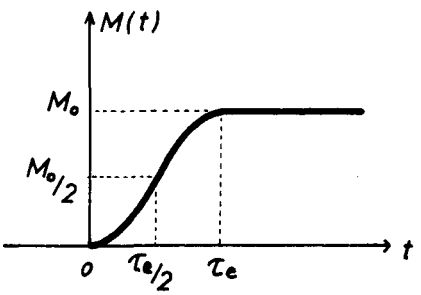

Fig. 6 A parabolic ramp function with rise time, τ_e and final moment, Mo assumed as a moment function.

$$e_{ij}=(U_{i,j}+U_{j,i})/2$$

$$U_{i,j}=-\frac{Mo}{4\pi\rho r^5}\left[\frac{1}{r^3}\cdot C_{ij}^{1}\,G(r,t)+\frac{1}{r^2}\left\{\frac{C_{ij}^{2p}}{\alpha^2}F''(t-t_\alpha)+\frac{C_{ij}^{2s}}{\beta^2}F''(t-t_\beta)\right\}+\frac{1}{r}\left\{\frac{C_{ij}^{3p}}{\alpha^3}F'''(t-t_\alpha)+\frac{C_{ij}^{3s}}{\beta^3}F'''(t-t_\beta)\right\}+\left\{\frac{C_{ij}^{4p}}{\alpha^4}F''''(t-t_\alpha)+\frac{C_{ij}^{4s}}{\beta^4}F''''(t-t_\beta)\right\}\right] \qquad (2)$$

where, $G(r,t)=\{F(t-t_\alpha)-F(t-t_\beta)\}/r+F'(t-t_\alpha)/\alpha-F'(t-t_\beta)/\beta$. $U_{i,j}$ denotes the differentiation of U_i component with respect to j axis and the suffix of i and j take all of x, y, and z. Coefficients of C_{ij}^{1} to C_{ij}^{4s} are summarized in Table 1. A parabolic ramp function was assumed as the moment function (Okada, 1975; Sasatani and Kasahara, 1978). The moment function, $M(t)$, is given by

$$M(t)/Mo=\frac{2}{\tau_e^2}t^2 \qquad \text{for} \quad 0\le t\le \tau_e/2$$

$$=1-\frac{2}{\tau_e^2}(\tau_e-t)^2 \qquad \text{for} \quad \tau_e/2\le t\le \tau_e$$

$$=1 \qquad \text{for} \quad t\ge\tau_e$$

as shown in Fig. 6. The rise time, τ_e, is approximately equivalent to the total

Table 1 A list of the coefficients needed in equation (2)

$U_{i,j}$	C^{1}_{ij}	C^{2P}_{ij}	C^{2S}_{ij}	C^{3P}_{ij}	C^{3S}_{ij}	C^{4P}_{ij}	C^{4S}_{ij}
Ux,x	$120x^3y-90xy^3$ $-90xyz^2$	$54x^3y-36xy^3$ $-36xyz^2$	$-51x^3y+39xy^2$ $+39xyz^2$	$14x^3y-6xy^3$ $-6xyz^2$	$-11x^3y+$ $9xy^3+9xyz^2$	$2x^3y$	$-x^3y+xy^3$ $+xyz^2$
Ux,y	$-24x^4+162x^2y^2$ $-18x^2z^2-24y^4$ $-18y^2z^2+6z^4$	$-10x^4+70x^2y^2$ $-8x^2z^2-10y^4$ $-8y^2z^2+2z^4$	$9x^4-69x^2y^2$ $+6x^2z^2+12y^4$ $+9y^2z^2-3z^4$	$-2x^4+16x^2y^2$ $-2x^2z^2-2y^4$ $-2y^2z^2$	$x^4-15x^2y^2$ $+4y^4+3y^2z^2$ $-z^4$	$2x^2y^2$	$-x^2y^2+y^4$ $+y^2z^2$
Ux,z	$180x^2yz-30y^3z$ $-30yz^3$	$78x^2yz-12y^3z$ $-12yz^3$	$-75x^2yz+$ $15y^3z+15yz^3$	$18x^2yz-2y^3z$ $-2yz^3$	$-15x^2yz+$ $5y^3z+5yz^3$	$2x^2yz$	$-x^2yz$ $+y^3z+yz^3$
Uy,x	$C^{1}_{xy}(x\leftrightarrow y)$	$C^{2P}_{xy}(x\leftrightarrow y)$	$C^{2S}_{xy}(x\leftrightarrow y)$	$C^{3P}_{xy}(x\leftrightarrow y)$	$C^{3S}_{xy}(x\leftrightarrow y)$	$C^{4P}_{xy}(x\leftrightarrow y)$	$C^{4S}_{xy}(x\leftrightarrow y)$
Uy,y	$C^{1}_{xx}(x\leftrightarrow y)$	$C^{2P}_{xx}(x\leftrightarrow y)$	$C^{2S}_{xx}(x\leftrightarrow y)$	$C^{3P}_{xx}(x\leftrightarrow y)$	$C^{3S}_{xx}(x\leftrightarrow y)$	$C^{4P}_{xx}(x\leftrightarrow y)$	$C^{4S}_{xx}(x\leftrightarrow y)$
Uy,z	$C^{1}_{xz}(x\leftrightarrow y)$	$C^{2P}_{xz}(x\leftrightarrow y)$	$C^{2S}_{xz}(x\leftrightarrow y)$	$C^{3P}_{xz}(x\leftrightarrow y)$	$C^{3S}_{xz}(x\leftrightarrow y)$	$C^{4P}_{xz}(x\leftrightarrow y)$	$C^{4S}_{xz}(x\leftrightarrow y)$
Uz,x	$180x^2yz-30y^3z$ $-30yz^3$	$78x^2yz-12y^3z$ $-12yz^3$	$-78x^2yz+$ $12y^3z+12yz^3$	$18x^2yz-2y^3z$ $-2yz^3$	$-18x^2yz+$ $2y^3z+2yz^3$	$2x^2yz$	$-2x^2yz$
Uz,y	$C^{1}_{zx}(x\leftrightarrow y)$	$C^{2P}_{zx}(x\leftrightarrow y)$	$C^{2S}_{zx}(x\leftrightarrow y)$	$C^{3P}_{zx}(x\leftrightarrow y)$	$C^{3S}_{zx}(x\leftrightarrow y)$	$C^{4P}_{zx}(x\leftrightarrow y)$	$C^{4S}_{zx}(x\leftrightarrow y)$
Uz,z	$C^{1}_{zx}(x\leftrightarrow z)$	$C^{2P}_{zx}(x\leftrightarrow z)$	$C^{2S}_{zx}(x\leftrightarrow z)$	$C^{3P}_{zx}(x\leftrightarrow z)$	$C^{3S}_{zx}(x\leftrightarrow z)$	$C^{4P}_{zx}(x\leftrightarrow z)$	$C^{4S}_{zx}(x\leftrightarrow z)$

$(\alpha\leftrightarrow\beta)$ indicates the interchange of α and β.

duration of faulting for an earthquake (Kanamori and Anderson, 1975) and is, therefore, called as "source process time" hereafter.

To evaluate the synthetic strain seismograms we assume an imaginary plane in an infinite medium so as to coincide with the ground surface (see Fig. 5). First, using equation (2), synthetic strain seismograms at an arbitrary point on the surface are calculated with parameters of the source location, the fault plane solution, the final seismic moment, and the source process time of an earthquake. In the calculation, P- and S-wave velocities which are calculated from the observed S-P time by assuming Poisson's ratio of 0.25 for the medium are used. Then, the synthetic strain seismograms are transformed into directions of actual extensometers installed to compare the observed strain seismograms directly. The free-surface effect is approximated by doubling the calculated amplitude. Okada (1980) has represented the exact solution of the strain field in a semi-infinite medium, in which we can see that our approximation is valid at least for the part of body waves. In the following analyses the initial part of body waves will mainly be investigated.

4. Comparison of observed and synthetic strain seismograms

Fig. 7 shows the first one of the strain seismograms observed by the newly improved recording system. The ordinal low chart-speed strain record is also shown in the upper-left corner of this figure. From this figure we can see that

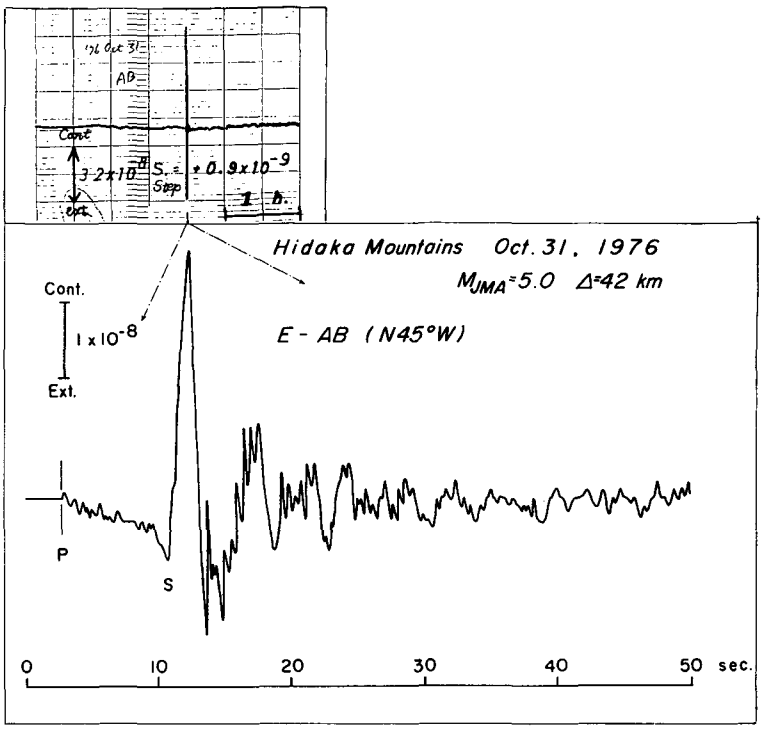

Fig. 7 The first strain seismogram observed by newly improved recording system.

the new system gives enough ability as a seismometer to the extensometer. The seismogram shows a considerably simple feature and smooth variation so that it seems to be no problem in the dynamic characteristics of the extensometer. This seismogram motivates us to analyze the observed strain fields for earthquakes.

To model the waveform of initial part of body waves in the observed strain seismogram the synthetic strain seismograms are computed for various sets of the source process time and the seismic moment. Best fitness between both seismograms provides the most probable source parameters of the event. We apply the waveform modeling analysis for 14 earthquakes observed from the beginning of July, 1976 to January, 1979. Fig. 8 shows the epicenters and the fault plane solutions of these earthquakes. Their hypocentral parameters, magnitudes, and epicentral distances to EGO are presented in Table 2. The event numbers in Table 2 will be refer to in the later figures. The fault plane solutions for the eight earthquakes from No. 4 to No. 11 were newly determined

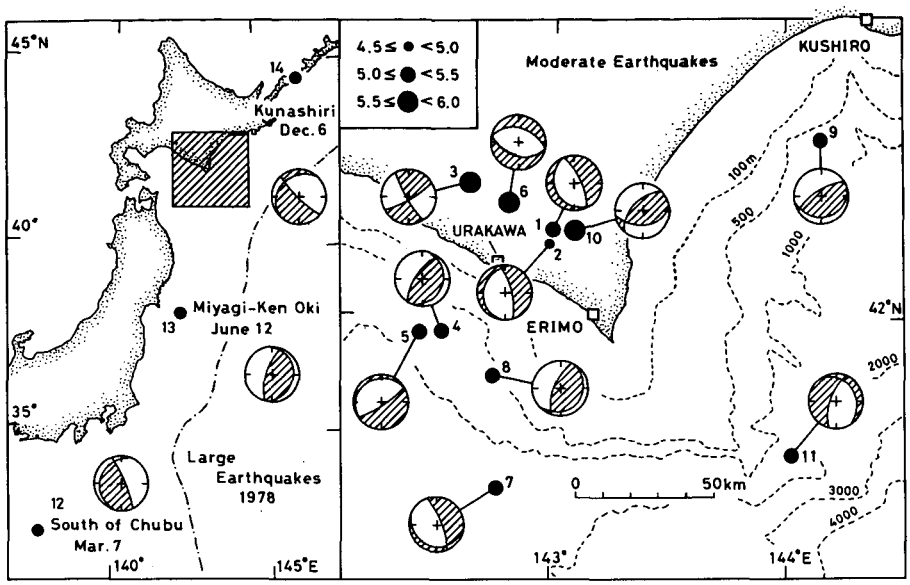

Fig. 8 Map showing epicenters and focal mechanism solutions for 14 earthquakes of which strain seismograms were compared with the synthetic ones. Numerals denote the earthquake numbers given in Table 2.

in this study on the basis of the P-wave first motion data obtained by the micro-earthquake observation networks of Hokkaido University, Tohoku University, and Hirosaki University together with JMA data. The P-wave first motion data on an equal area projection of the upper focal hemisphere for the eight earthquakes are shown in Fig. 9, in which the nodal lines are also shown. For three earthquakes from No. 1 to No. 3 fault plane solutions given by Sasatani and Kasahara (1978) were used. Those for three large earthquakes from No. 12 to No. 14 given by Sudo and Ishibashi (1978), Seno et al. (1980), and Sudo and Sasatani (1979) were referred to. The last largest earthquake, No. 14, has been analyzed in detail by the same method mentioned above (Kasahara and Sasatani, 1985). The result only is used in this article.

4.1 Hidaka Mountains earthquake of October 31, 1976.

Fig. 10 shows the observed strain seismograms and the optimal synthetic ones for the 1976 Hidaka Mountains earthquake (Sasatani and Kasahara, 1978). Waveform showing a one-directional drift from P to S wave arrivals, which cannot be recorded by pendulum type seismometers, is explained by a near field term in equation (2). As shown in the figure, the agreement is quite good

Table 2 List of earthquakes of which strain seismograms are analyzed in this study.

No.	Date			Time		Lat. °N	Long. °E	H. km	△ km	M_{JMA}	e_s 10^{-9}	τ_e sec	Moment dyne・cm
	y	m	d	h	m								
1	76	10	31	21	30	42.37	142.98	61	42	5.0	38	4.1	2.1×10^{24}
2		11	1	15	5	42.32	142.98	60	37	4.7	19	2.7	4.4×10^{23}
3	77	2	24	20	40	42.49	142.60	47	70	6.0	174	3.8	9.5×10^{24}
4		5	6	7	14	41.97	142.45	75	59	5.2	18	1.9	2.7×10^{23}
5		11	17	4	36	41.97	142.34	78	68	5.3	16	1.8	2.4×10^{23}
6	78	3	20	16	19	42.42	142.78	77	55	5.5	85	2.8	2.8×10^{24}
7		4	6	17	39	41.39	142.68	51	80	5.1	9	2.9	3.2×10^{23}
8		7	16	2	44	41.79	142.67	67	47	5.3	210	2.1	3.4×10^{24}
9		10	29	7	46	42.59	144.30	80	115	5.3	18	2.6	7.7×10^{23}
10		11	7	0	8	42.31	143.08	61	34	5.5	148	1.9	1.7×10^{24}
11	79	1	19	20	56	41.47	144.12	39	94	5.4	94	3.6	1.2×10^{25}
12	78	3	7	11	48	31.90	137.77*	440	1200	6.9	59	7.6	2.0×10^{26}
13		6	12	17	14	38.15	142.17*	40	445	7.4	329	13.1	1.1×10^{27}
14		12	6	23	3	44.12	146.94	168	387	7.7	235	45.0	9.0×10^{27}
15	76	11	4	20	20	42.32	144.19	63	92	4.5	5	1.5	5.1×10^{22}
16		11	8	17	19	38.07	142.32*	30	440	6.2	17	3.9	5.1×10^{24}
17	77	6	5	15	41	42.26	142.97	49	33	4.7	8	1.0	2.1×10^{22}
18	78	3	25	4	47	44.33	149.82*	40	620	7.3	287	14.0	1.6×10^{27}
19		5	16	16	35	40.95	141.47*	10	204	5.8	12	3.6	1.4×10^{24}
20		5	16	17	23	40.93	141.45*	10	204	5.8	27	3.1	2.3×10^{24}
21		6	21	20	10	47.68	149.23*	380	818	6.7	27	4.5	2.2×10^{25}
22	79	2	20	15	32	40.22	143.87*	0	234	6.5	213	7.0	1.1×10^{26}
23		4	24	17	5	41.41	142.10	89	111	5.2	47	2.4	1.7×10^{24}

Table 2 Continued.

No.	Date			Time		Lat. °N	Long. °E	H. km	△ km	M_{JMA}	e_s 10^{-9}	τ_e sec	Moment dyne • cm
	y	m	d	h	m								
24	79	5	26	6	11	42.30	143.00	61	32	4.9	32	1.4	1.9×10^{23}
25		10	22	16	3	41.97	142.33	79	69	4.3	6	1.1	3.2×10^{22}
26		12	7	3	29	42.03	142.56	67	49	3.6	4.2	0.56	4.9×10^{21}
27		12	7	4	58	40.72	144.92	72	207	4.4	11	0.73	5.9×10^{22}
28		12	14	16	19	42.83	144.28	44	129	5.7	169	2.0	4.1×10^{24}
29		12	14	21	50	41.16	142.76	31	101	3.6 #	6.1	0.63	1.2×10^{22}
30		12	21	19	51	42.14	143.37	45	22	3.3 #	3.2	0.37	9.9×10^{20}
31		12	25	6	7	42.43	143.89	49	76	4.0	23	0.60	3.4×10^{22}
32	80	2	14	21	1	40.18	142.15*	40	228	4.1	3.8	0.60	1.4×10^{22}
33		2	15	13	51	41.42	142.77	50	91	4.1	13	0.74	3.1×10^{22}
34		2	15	23	25	44.77	149.83*	50	632	5.7	15	5.6	1.3×10^{25}
35		2	16	0	0	44.57	149.65*	0	651	5.5	10	3.3	3.2×10^{24}
36		2	18	15	8	43.55	146.04	129	235	5.6	20	0.93	2.5×10^{23}
37		2	19	10	33	41.63	142.10	65	98	4.7	23	0.86	9.0×10^{22}
38		2	25	7	39	41.94	142.31	80	71	3.7	5.1	0.60	8.8×10^{21}
39		2	25	15	45	42.65	142.94	106	72	4.5	33	0.79	1.2×10^{23}
Aftershock sequence													
Mainshock													
40	80	2	23	14	51	43.46	146.73	30 $	333	6.8	300	5.4	1.3×10^{26}
Aftershocks													
41		2	23	15	50	43.42	147.02	30 $	353	5.7	67	2.2	5.1×10^{24}
42		2	24	3	55	43.69	146.57	30 $	335	4.5	2.1	0.84	2.2×10^{22}
43		2	24	7	39	43.15	147.14	30 $	350	5.9	80	2.3	6.7×10^{24}
44		2	24	11	27	43.15	147.26	30 $	360	5.0	11	1.7	5.1×10^{23}
45		2	24	11	44	43.21	147.25	30 $	362	4.9	2.0	1.0	3.2×10^{22}

Table 2 Continued.

No.	Date			Time		Lat. °N	Long. °E	H. km	△ km	M_{JMA}	e_s 10^{-9}	τ_e sec	Moment dyne • cm
	y	m	d	h	m								
46	80	2	24	12	13	43.11	147.31	30 $	363	4.6	2.5	1.1	4.9×10^{22}
47		2	24	12	21	43.09	147.29	30 $	358	4.8	3.8	0.84	4.4×10^{22}
48		2	24	13	38	43.76	146.99	30 $	368	4.7	4.7	1.1	9.4×10^{22}
49		2	24	21	33	43.18	147.45	30 $	376	4.8	3.6	1.8	1.9×10^{23}
50		2	25	0	32	43.21	148.31	30 $	440	4.8	3.4	1.6	1.7×10^{23}
51		2	26	7	39	43.41	148.00	30 $	437	4.5	1.3	1.5	5.8×10^{22}
52		2	26	18	56	43.29	147.15	30 $	356	5.0	4.4	1.7	2.1×10^{23}
53		2	27	21	45	43.27	146.86	30 $	334	5.7	57	2.1	3.7×10^{24}
54		2	28	8	3	43.25	146.88	30 $	335	5.4	17	1.4	5.0×10^{23}
55		3	1	7	46	43.51	146.73	30 $	337	4.6	3.4	0.84	3.6×10^{22}

Focal parameters are determined by the Research Center for Earthquake Prediction, Hokkaido University excluding those with * mark, which are determined by Japan Meteorological Agency (JMA).
e_s and τ_e are average amplitude and period of the first S-waves in the observed strain seismograms by three components of extensometers. Seismic moment estimated from the equation (5) is listed for each event.
Magnitede with # is estimated from F-P time.

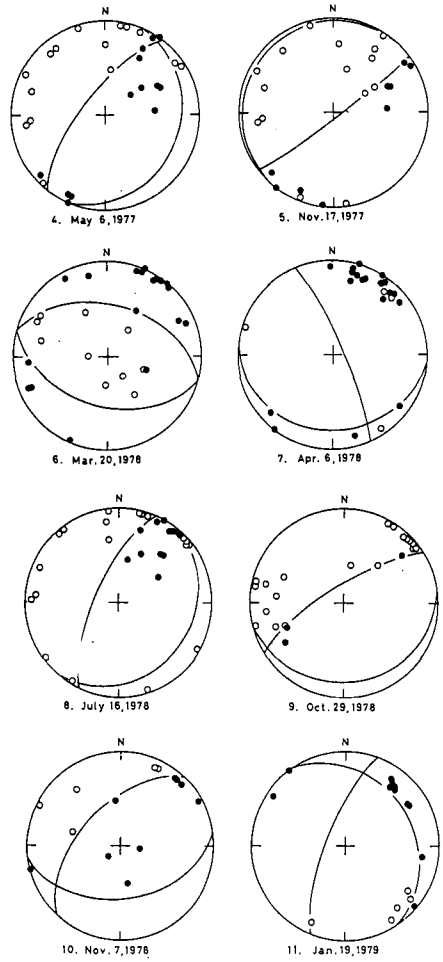

Fig. 9 Focal mechanism solutions for eight earthquakes which were newly obtained in this study. Numbers correspond to events in Table 2. Equal area projection (upper hemisphere) of the P-wave first-motion data are shown. Solid and open circles indicate compressional and dilatational first-motions, respectively.

between the observed and synthetic waveforms including the one-directional drift. This agreement suggests that the extensometer with a solid length standard 30 meters long can satisfactorily respond to a short-period crustal strain change up to an amount of 1 part in 10^9. The seismic moment obtained (3.5×10^{23} dyne cm) is consistent with that predicted by the empirical relation between *Mo* and *M* (Hanks and Kanamori, 1979).

4.2 Off Erimo earthquake of January 19, 1979.

Fig. 11 shows an example of the strain seismograms for the shallow event (No. 11) with an epicentral distance of 94 kilometers. The seismograms show

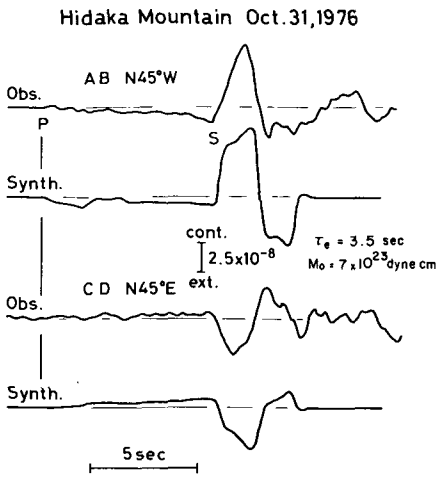

Fig. 10 Comparison of the observed strain seismograms with the optimal synthetic ones for the Hidaka Mountains earthquake of October 31, 1976.

a remarkable phase arriving between the P- and S-waves. This phase may correspond to SP-wave, which is expected for the semi-infinite medium (Okada, 1980). Except the SP-wave which is not taken into account in our calculation, a good agreement was obtained between the observed and synthetic records for both the P-wave and the initial part of S-wave in the case of the source process time of 3.0 seconds.

4.3 South of Chubu earthquake of March 7, 1978.

Fig. 12 shows a strain seismogram obtained for the deep-focus earthquake of March 7, 1978 in the south of Japan which is located at about 1,200 kilometers

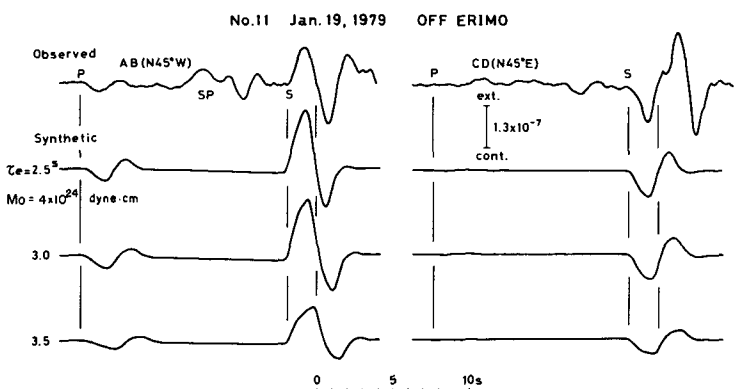

Fig. 11 Observed strain seismograms and synthetic ones calculated for various values of source process time τ_e for off Erimo earthquake of January 19, 1979.

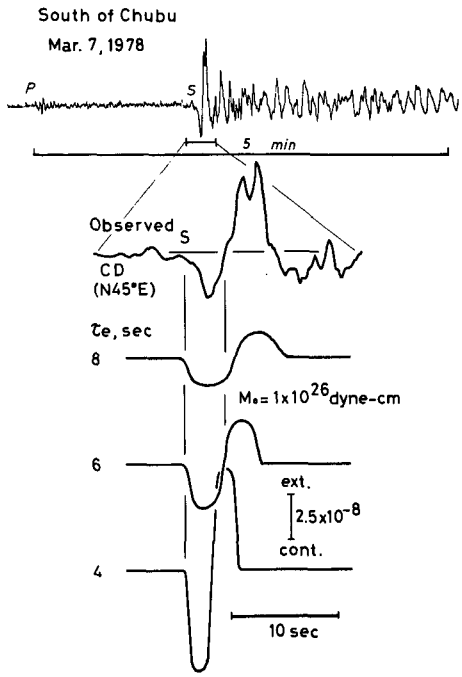

Fig. 12 Observed strain seismogram of the South of Chubu earthquake of March 7, 1978 (upper part) and comparison of the S-wave part between observed and synthetic strain seismograms calculated for various values of source process time τ_e.

southwest of the EGO (see left in Fig. 8). The first one-cycle of S-wave in the seismogram seems to be simple in waveform. In the lower of the figure, the waves for about 25 seconds which include the S-wave are expanded in time, with which three synthetic strain seismograms are also shown. Since the epicentral distance is too large to allow the method of synthesis mentioned in the previous section, we used that for the far-field body waves (e.g., Sasatani, 1980). These synthetic strain seismograms were calculated for different source process times (τ_e) of 8, 6, and 4 seconds with a seismic moment of 1×10^{26} dyne•cm. From comparison of waveform and the amplitudes between the observed and synthetic seismograms, the source process time (τ_e) was obtained to be 6 sec and the seismic moment (Mo), 1.0×10^{26} dyne•cm.

4.4 Miyagi-ken Oki earthquake of June 12, 1978.

The upper part of Fig. 13 shows two components of the strain seismograms obtained for the shallow event with a magnitude of 7.4 which occurred off Miyagi Prefecture on June 12, 1978. As shown in the figure, the seismograms record remarkably predominant surface waves immediately after the S-wave arrival, so that only the first half cycle of the S-wave could be taken for

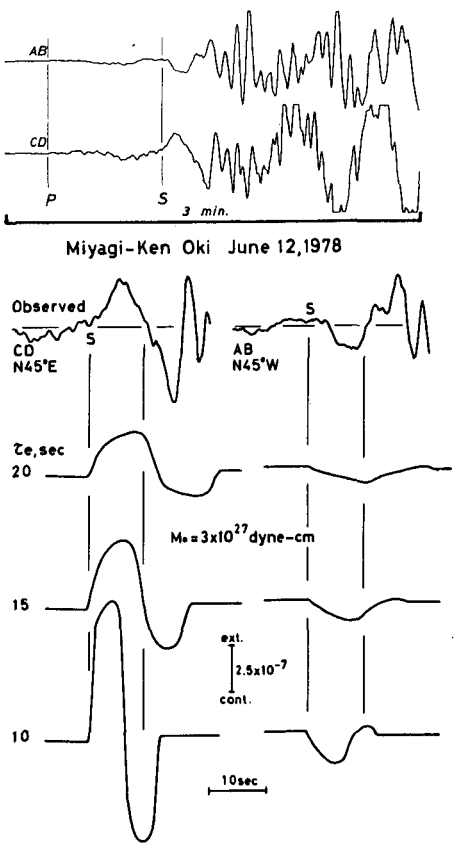

Fig. 13 Observed and synthetic strain seismograms for the Miyagi-ken-oki earthquake of june 12, 1978.

comparison with the synthetic seismograms. Three examples of synthetic strain seismograms for the S-wave are also shown in the lower part of the figure in comparison with the observed ones. Among these synthetic seismograms, the second ones are the most similar to the observed ones. Then, we estimated that the seismic moment (Mo) and the source process time (τ_e) are 3×10^{27} dyne · cm and 15 sec, respectively. These values are nearly the same as those obtained by Seno et al. (1980), in which the seismic moment is 3.1×10^{27} dyne · cm and the source process time is estimated as about 15 sec from their one segment model.

4.5 The other earthquakes.

Fig. 14 (a) and (b) show the strain seismograms for ten near-by earthquakes. These earthquakes were classified into two groups depending on their source regions. If the ratio of the epicentral distance to the focal depth is less than the critical value for the appearance of SP-wave, the observed strain seismograms are expected to show very simple features. Since the earthquakes occurring under the southern part of Hidaka range have this condition for EGO, fairly good agreement between the observed and synthetic strain seismograms may be obtained as shown in Fig. 14 (a). On the other hand, strain seismograms of the events which occurred off Urakawa and Kushiro are rather complicated (Fig. 14 (b)). However, the observed and synthetic strain seismograms give fairly good agreement so long as S-wave are taken for these earthquakes.

4.6 Relation between the seismic moments deduced from strain seismograms and those from the other method.

The seismic moments determined through these analyses are plotted in Fig. 15 with respect to those obtained by other methods. Seismic moment shown by solid and open circles are estimated from conventional seismological method (Sasatani and Kasahara, 1978 ; Seno et al., 1980 ; Sudo and Sasatani, 1979) and from the empirical relation between magnitude and seismic moment (Hanks and Kanamori, 1979), respectively. This figure shows that the seismic moment estimated from the strain seismogram is consistent with that from other methods within a factor 2 except a few moderate earthquakes. A little large difference for a few moderate events may be caused by complex waveform of the observed strain seismogram and also the simple model used in the analysis.

5. Estimation of source parameters from S-wave of strain seismogram and its applications.

5.1 Theoretical consideration

Simple waveform allows us to apply the following analysis to the observed strain seismograms. The previous analyses show that the period of S-wave is very sensitive to the source process time and the amplitude of the wave depends on the seismic moment ; therefore, quantitative investigation of S-wave form of the observed strain seismogram provides the source parameters.

As far as the parabolic ramp function is adopted as the moment function, at

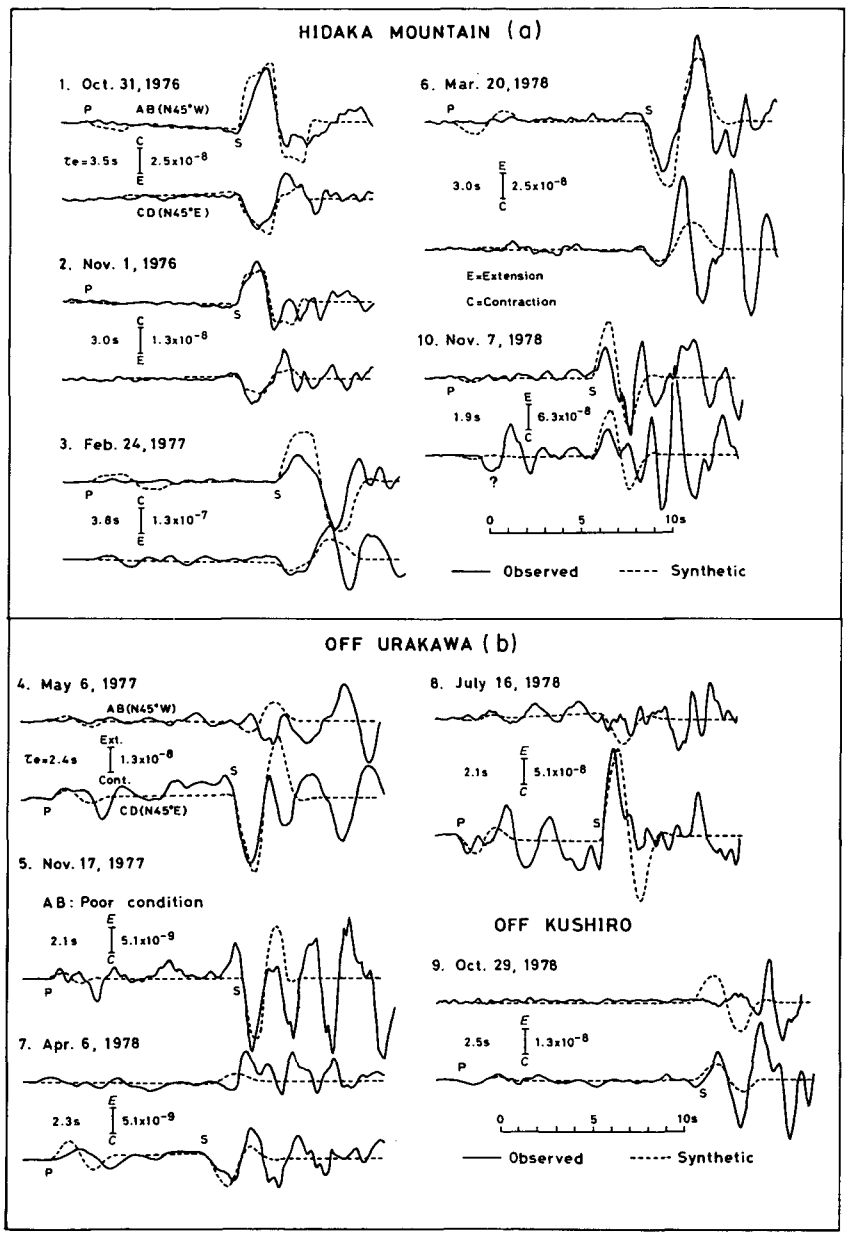

Fig. 14 Comparison of the observed strain seismograms with the optimal synthetic ones for the earthquakes occurring near EGO.

a far field, a period of S-wave corresponds theoretically to the source process time, τ_e, and the amplitude of S-wave, e, is related to the last term in equation (2); that is,

$$e=\frac{Mo}{\pi\rho r}\frac{Rc}{\beta^4}\frac{2}{\tau_e{}^2} \tag{3}$$

where Rc is the constant due to the radiation pattern and e is peak to peak amplitude. The amplitude of S-wave, e_s, observed at the free surface is approximated by the equation, $e_s=2e$. Then, the seismic moment Mo is obtained as

$$Mo=\frac{\pi\rho\beta^4}{4Rc}e_s r\tau_e{}^2. \tag{4}$$

This equation suggests that the seismic moment can be estimated easily from the period and amplitude of S-wave of the observed strain seismogram if the distance from the source to station is given.

Fig. 16 shows logarithmic plots of the seismic moments obtained by the method described in the previous section as a function of the product of the distance r, the amplitude e_s and the square of the period τ_e of the observed strain seismograms. The amplitude and the period were obtained from the

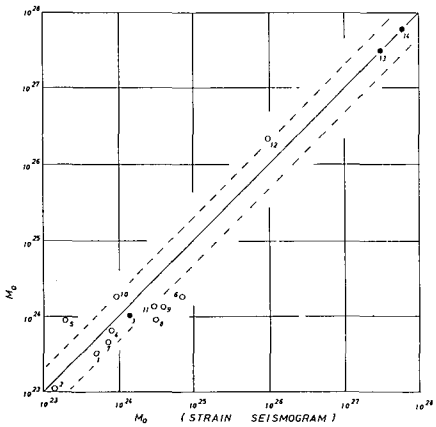

Fig. 15 Plot of seismic moments estimated from strain seismograms versus those obtained by the conventional seismological method (solid circle) and estimated from the empirical relationship between magnitude and seismic moment (open circle).

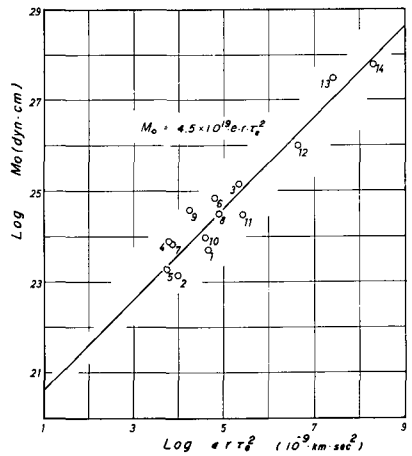

Fig. 16 The relationship between seismic moments and a product of S-wave amplitude (e), a second power of period of S-wave ($\tau_e{}^2$) and a hypocentral distance (r).

mean value for the three components of the strain seismograms. The distance, r, was calculated by $(\Delta^2+H^2)^{1/2}$ where Δ is the epicentral distance and H is the focal depth. From these plots the constant, $\pi\rho\beta^4/4Rc$, in equation (4) was determined to be 4.5×10^{19}, that is, the seismic moment Mo in dyne•cm can be obtained from the equation,

$$Mo=4.5\times10^{19}e_s r\tau_e^2, \tag{5}$$

where e_s is measured in 1 part in 10^9, r in kilometers and τ_e in seconds. A straight line in Fig. 16 gives this relation. The figure shows that the seismic moment within a factor 2 can be determined from the amplitude and period of S-wave of the observed strain seismogram and the hypocentral distance even if the fault plane solution of the event is not given. Using equation (5), the seismic moments as well as the source process times of other 11 earthquakes occurring from February to November in 1979 have been estimated. These parameters obtained and the amplitude and period of observed S-wave are also summarized in Table 2.

5.2 Strain seismograms of small earthquakes

The waveform of the observed strain seismograms may directly reflect the source parameters as mentioned above. This favorable relation stimulates us to improve the extensometer to be more sensitive. For the purpose, a new channel with a sensitivity of 1.13×10^{-10}/bit in the frequency range of 0.01 Hz to 3 Hz was equipped and the observation has been carried out by the E-AB component from December, 1979. During the total 40 days till the end of February, 1980 (excluding no observation period for 50 days due to failure of the system by thunder) 32 earthquakes were recorded (see Fig. 1).

The middle part of Fig. 17 shows the strain seismogram of the smallest earthquake with a magnitude of 3.3 among all of the observed earthquakes. Other seismograms observed by short-period horizontal seismometers (the natural period 1 Hz) which were applied to a low-pass filter with a short-period cut-off at 3 Hz are also shown in the upper and lower parts in this figure. We cannot compare with each other in detail, because both instruments are installed in different directions. However, it can be seen that main features of both seismograms are very similar. A scale of 1 micron meter of ground displacement at 3 Hz is shown for comparison. As shown in the figure, the observed amplitudes are also in good agreement. Therefore, this figure indicates that the extensometer can sufficiently respond to short-period crustal strain variations up to 3 Hz. Fig. 18 shows the strain seismograms for four small earthquakes.

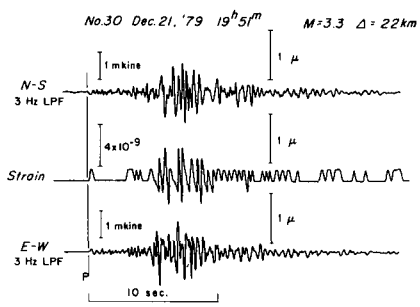

Fig. 17 Comparison of the observed strain seismogram for the earthquake with the smallest magnitude in this study (middle part) with the low-pass filtered seismograms observed by short-period horizontal seismometers (upper and lower parts).

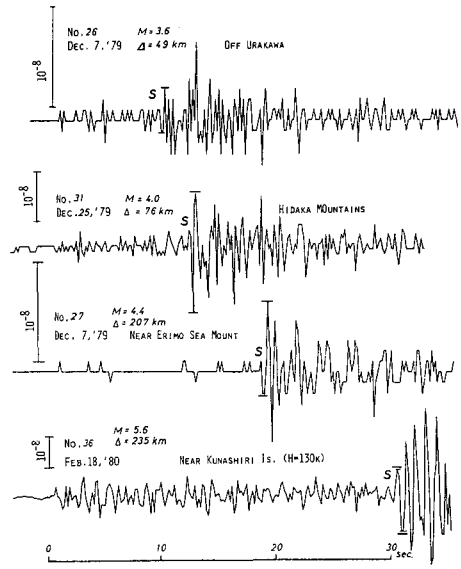

Fig. 18 Examples of strain seismograms for small earthquakes. The first one-cycle of S-wave is shown by a pair of short horizontal lines. Event numbers refer to Table 2.

Seismic moments and source process times of these small earthquakes have also been determined from amplitudes and periods of the first S-waves by using equation (5). These quantities determined are also summarized in Table 2.

5.3 Relationship between seismic moments and source process times

Seismic moments Mo are plotted against source process time τ_e in Fig. 19, in which solid marks are obtained in the present study and open ones obtained by conventional seismological method. All of the results obtained by the present study are listed in Table 2 and others, which are referred to the source parameters summarized by Geller (1976) and to the new ones obtained by Abe (1978), are listed in Table 3. In Fig. 19 circle and triangle marks correspond to uni-lateral and bi-lateral rupture modes, respectively. The results obtained from strain seismograms are consistent with those by the other method over the wide range of seismic moment. Two lines in this figure show the theoretical relations obtained by assuming rectangular fault model and similarity conditions with an average rupture velocity of 2.5 km/sec and a stress drop of 30 bars for shallow earthquakes (Abe, 1975; Geller, 1976). This figure demonstrates

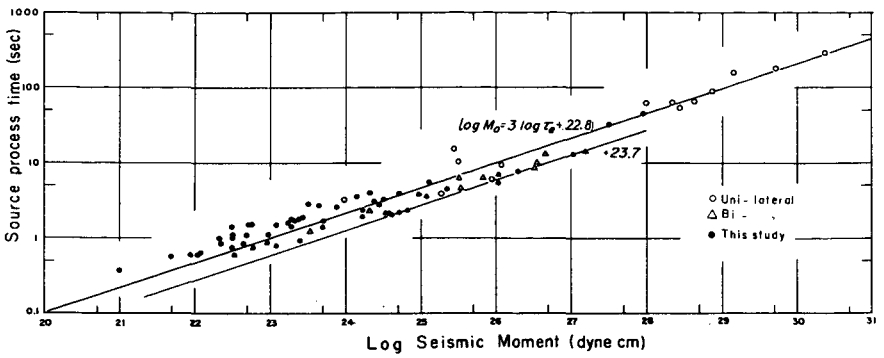

Fig. 19 Plot of source process times versus seismic moments. The open circle and triangle denote uni-lateral and bi-lateral rupture modes obtained by conventional seismological method (Table 3), and the solid circles denote the results obtained in this study (Table 2). Two straight lines are calculated by the assumed fault parameters (see text).

Table 3 List of seismic moment and source process time data obtained by conventional seismological method and other related parameters

		Date			Moment dyne·cm	τ_e* sec	L. km	Vr. km/s	Mode	Ref.#
		y	m	d						
1	Tango	27	3	27	4.6×10^{26}	7.6	35	2.3	B	G
2	Saitama	31	9	21	6.8×10^{25}	4.3	20	2.3	B	G
3	Sanriku	33	3	2	4.3×10^{28}	58	185	3.2	U	G
4	Long Beach	33	3	11	2.8×10^{25}	13−6.5	30	2.3	?	G
5	South Izu	34	3	21	9.5×10^{23}	2.3	7	3.0	U	A
6	Tottori	43	9	10	3.6×10^{26}	7.2	33	2.3	B	G
7	Fukui	48	6	28	3.3×10^{26}	6.5	30	2.3	B	G
8	Chili	60	5	22	2.4×10^{30}	230	800	3.5	U	G
9	Kitamino	61	8	19	9.0×10^{25}	4.0	12	3.0	U	G
10	Wakasawan	63	3	27	3.3×10^{25}	4.3	20	2.3	B	G
11	Kurile	63	10	13	7.5×10^{28}	71	250	3.5	U	G
12	Alaska	64	3	28	5.2×10^{29}	143	500	3.5	U	G
13	Rat Island	65	2	4	1.4×10^{29}	125	500	4.0	U	G
14	Parkfield	66	6	28	3.2×10^{25}	9.6	26	2.7	U	G
15	Tokachioki	68	5	16	2.8×10^{28}	43	150	3.5	U	G
16	Saitama	68	7	1	1.9×10^{25}	2.9	10	3.4	U	G
17	Kurile	69	8	11	2.2×10^{28}	51	180	3.5	U	G
18	Gifu	69	9	9	3.5×10^{25}	3.4	18	2.5	U	G
19	Peru	70	5	31	1.0×10^{28}	52	130	2.5	U	G
20	San Fernando	71	2	9	1.2×10^{26}	8.3	20	2.4	U	G
21	Amagi	74	7	9	3.2×10^{23}	0.6	3.5	3.0	B	A
22	Kawazu	76	8	17	2.1×10^{24}	1.9	9	2.4	B	A

*τ_e is calculated from L/Vr · n (n=1 for Uni-lataral, =2 for bi-lateral).
Ref. G: Geller (1976), A: Abe (1978).

that the extensometer with a solid length standard 30 meters long is extremely excellent as a seismometer because of capability to respond to crustal movement in frequency range of 3 Hz to DC. In addition to the capability, the observable magnitude range can be extended, if the extensometer is used.

6. Concluding remarks

The digital system newly improved for the extensometric observation observed strain seismograms of 55 earthquakes with magnitudes ranging from 3.3 of 7.7 of which body wave analyses were applied on the basis of the theoretical strain seismogram generated by a point shear dislocation in an infinite homogeneous medium. The waveform and amplitude of the observed strain seismogram in the initial part of body waves could be well modeled by the synthetic strain seismogram calculated for the source parameters which were consistent with those obtained by conventional seismological methods within a factor 2. Seismic moment and source process time of an earthquake could be estimated from amplitude and period of the observed S-wave alone because the extensometer system used here had no transient characteristics. Source process time ranging from 0.3 to 60 seconds and seismic moment ranging from 10^{20} to 10^{27} dyne•cm were obtained from the analyses of the observed strain seismograms for 55 earthquakes. The relation between both parameters was also consistent with that predicted by the earthquake dislocation model. The results obtained by analyses of strain seismograms confirmed that the extensometer can satisfactorily respond to crustal strain variations in the frequency range from 3 Hz to DC component caused by earthquakes and demonstrated the superiority of the extensometer as a seismometer, when it was utilized in conjunction with the available digital recording system.

Acknowledgements

One of the authors, M.K., would like to express my gratitude to Professor Izumi Yokoyama of Geophysical Institute, Hokkaido University for giving the opportunity of this study and for his continuous support and encouragement during the course of this study. We are also very grateful to Professor Hiroshi Okada of Geophysical Institute, Hokkaido University who made many valuable suggestions and kindly reviewed the manuscript and to Dr. Katsuyuki Abe of Earthquake Research Institute, Tokyo University for his useful discussion on source parameters and his encouragement. We are thankful to the members of

the Research Center for Earthquake Prediction, Hokkaido University for helpful discussions and to the Seismological Observatories of Tohoku and Hirosaki Universities for providing the P-wave first motion data. Thanks are also due to Mr. Yasumori Tanaka for his efforts to routine observation at the Erimo Geophysical Observatory and to Dr. Juhei Yamada of ex. Earthquake Research Institute, Tokyo University for his consulting to construction of the observatory. This work also greatly benefited from discussios with Dr. Yoshimitsu Okada of National Research Center for Disaster Prevention.

References

Abe, K., 1975. Reliable estimation of the seismic moment of large earthquakes. J. Phys. Earth, **23**, 381-390.

Abe, K., 1978. Dislocations, source dimentions and stresses associated with earthquakes in the Izu Peninsula, Japan. J. Phys. Earth, **26**, 253-274.

Benioff, H., 1935. A linear strain seismograph. Bull. Seism. Soc. Am., **25**, 283-309.

Benioff, H., 1959. Fused-quartz extensometer for secular, tidal, and seismic strains. Bull. Geol. Soc. Am., **70**, 1019-1032.

Berger, J. and Wyatt, F., 1973. Some observations of Earth strain tides in California. Phil. Trans. R. Soc. London A, **274**, 267-277.

Blayney, J.L. and Gilman, R., 1965. A portable strainmeter with continuous interferometric calibration. Bull. Seism. Soc. Am., **55**, 955-970.

Chung, W.Y. and Kanamori, H., 1978. Subduction process of a fracture zone and aseismic ridges—the focal mechanism and source characteristics of New Hebrides earthquake of 1969 January 19 and some related events. Geophys. J.R. astr. Soc., **54**, 221-240.

Fukao, Y. and Furumoto, M., 1975. Mechanism of large earthquakes along the eastern margin of the Japan sea. Tectonophysics, **26**, 247-266.

Funahashi, M. and Hashimoto, S., 1951. Geology of the Hidaka zone, Hokkaido. Monograph of the association for the geological collaboration, **No. 6**, 38pp (in Japanese).

Geller, R.J., 1976. Scaling relations for earthquake source parameters and magnitudes. Bull. Seism. Soc. Am., **66**, 1501-1523.

Hanks, T.C. and Kanamori, H., 1979. A moment magnitude scale. J. Geophys. Res., **84**, 2348-2350.

Honda, H., 1962. Earthquake mechanism and seismic waves. J. Phys. Earth, **10**, 1-97.

Maeda, J., Motoya, Y. and Suzuki, S., 1978. On the telemetered data recording and processing system for earthquakes and Earth strains at Hokkaido University. Zisin (Bull. Seism. Soc. Jap.), Ser. II, **31**, 401-413 (in Japanese with English abstract).

Maruyama, T., 1963. On the force equivalences of dynamical elastic dislocations with reference to the earthquake mechanism. Bull. Earthq. Res. Inst., **41**, 467-486.

Kanamori, H., 1972. Mechanism of tsunami earthquakes. Phys. Earth Planet. Interiors, **6**, 346-359.

Kanamori, H. and Anderson, D.L., 1975. Theoretical basis of some empirical relations in seismology. Bull. Seism. Soc. Am., **65**, 1073-1095.

Kanamori, H. and Cipar, J.J., 1974. Focal process of the great Chilean earthquake of May 22, 1960. Phys. Earth Planet. Interiors, **9**, 128-136.

Kanamori, H. and Stewart, G.S., 1979. A slow earthquake. Phys. Earth Planet. Interiors, **11**, 312-332.

Kasahara, M., 1976. Seismic and geodetic observations through the digital PCM telemetering system in Hokkaido, Japan. J. Geod. Soc. Jap., **22**, 292-294.

Kasahara, M. and Sasatani, T., 1985. Source characteristics of the Kunashiri strait earthquake of December 6, 1978 as deduced from strain seismograms. Phys. Earth Planet. Interiors, **37**, 124-134.

Okada, Y., 1975. Theoretical strain seismogram (1). Abstr. Annu. Meet. Seism. Soc. Jap., No. 1, 240, (in Japanese).

Okada, Y., 1980. Theoretical strain seismogram and its applications. Bull. Earthq. Res. Inst., **55**, 169-182 (in Japanese with English abstract).

Okada, Y., Watanabe, S. and Kasahara, K., 1975. Observation of crustal deformation at the Fujigawa Observatory, Central Honshu, Japan (1). J. Geod. Soc. Jap., **21**, 179-190 (in Japanese with English abstract).

Sacks, I.S., Suehiro, S., Linde, A.T. and Snoke, J.A., 1978. Slow earthquakes and stress redistribution. Nature, **275**, 599-602.

Sasatani, T., 1980. Source parameters and rupture mechanism of deep-focus earthquakes. J. Fac. Sci. Hokkaido Univ., Ser. VII (Geophysics), **6**, No. 2, 301-384.

Sasatani, T. and Kasahara, M., 1978. Analyses of strain seismograms from near earthquakes. Zisin (Bull. Seism. Soc. Jap.), Ser. II, 31, 11-23 (in Japanese with English abstract).

Seno, T., Shimazaki, K., Somerville, P., Sudo, K. and Eguchi, T., 1980. Rupture process of the Miyagi-oki, Japan, Earthquake of June 12, 1978. Phys. Earth Planet. Interiors, **23**, 39-61.

Sudo, K. and Ishibashi, K., 1978. Source process of the deep-focus earthquake of March 7, 1978 beneath the Ogasawara Islands. Abstr. Annu. Meet. Seism. Soc. Jap., No. 1, 98, (in Japanese).

Sudo, K. and Sasatani, T., 1979. Source mechanism of the Earthquake of December 6, 1978 beneath Etorofu Island (M=7.7). Abstr. Annu. Meet. Seism. Soc. Jap., No. 1, 31, (in Japanese).